Reprinted from

JAPANESE JOURNAL OF
APPLIED
PHYSICS

REGULAR PAPER

Noninvasive Measurement of Transient Change in Viscoelasticity Due to Flow-Mediated Dilation Using Automated Detection of Arterial Wall Boundaries

Kazuki Ikeshita, Hideyuki Hasegawa, and Hiroshi Kanai

Jpn. J. Appl. Phys. **50** (2011) 07HF08

Japanese Journal of Applied Physics **50** (2011) 07HF08 **REGULAR PAPER**
DOI: 10.1143/JJAP.50.07HF08

Noninvasive Measurement of Transient Change in Viscoelasticity Due to Flow-Mediated Dilation Using Automated Detection of Arterial Wall Boundaries

Kazuki Ikeshita[1]*, Hideyuki Hasegawa[1,2], and Hiroshi Kanai[2,1]

[1]*Graduate School of Biomedical Engineering, Tohoku University, Sendai 980-8579, Japan*
[2]*Graduate School of Engineering, Tohoku University, Sendai 980-8579, Japan*

Received December 13, 2010; accepted March 7, 2011; published online July 20, 2011

We measured the stress–strain relationship of the radial arterial wall during a heartbeat noninvasively. In our previous study, the viscoelasticity of the intima–media region was estimated from the stress–strain relationship, and the transient change in viscoelasticity due to flow-mediated dilation (FMD) was estimated. In this estimation, it is necessary to detect the lumen–intima boundary (LIB) and the media–adventitia boundary (MAB). To decrease the operator dependence, in the present study, a method is proposed for automatic and objective boundary detection based on template matching between the measured and adaptive model ultrasonic signals. Using this method, arterial wall boundaries were appropriately detected in *in vivo* experiments. Furthermore, the transient change in viscoelasticity estimated from the stress–strain relationship was similar to that obtained manually. These results show the feasibility of the proposed method for automatic boundary detection enabling an objective and appropriate analysis of the transient change in viscoelasticity due to FMD.

1. Introduction

The quantitative assessment of atherosclerosis, which is the main cause of circulatory diseases, is essential for making an early diagnosis of such diseases. In early-stage atherosclerosis, endothelial dysfunction occurs.[1,2] Additionally, it has been reported that the characteristics of the smooth muscle that composes the media of the artery change owing to atherosclerosis.[3] Consequently, it is important for an early preventive treatment to noninvasively assess the endothelial function and mechanical properties of the media mainly composed of the smooth muscle.

The intima, the innermost layer, is composed of endothelial cells and an internal elastic membrane. The endothelial cells produce the endocrine substances for maintaining the homeostasis of the vascular system.[4] The smooth muscle that composes the media is the main source of the viscoelasticity of the vessel wall. Therefore, the dilation and contraction of the artery depend on the characteristics of the media. Endothelial cells react to the shear stress caused by blood flow and produce nitric oxide (NO), which is known as a vasodepressor. The smooth muscle in the media is relaxed as a result of the response to the produced NO.

For the evaluation of the endothelial function, a conventional technique is used to measure the transient change in the inner diameter of the brachial artery caused by flow-mediated dilation (FMD) after the release of avascularization.[5–9] However, this method cannot directly evaluate the mechanical properties of the arterial wall. Additionally, the increase in the inner diameter of the brachial artery is very small (about 0.4 mm) compared with the spatial resolution of conventional ultrasonic diagnostic equipment of 0.1 mm.[10] Therefore, we have developed a method of directly measuring the changes in the elasticities of the intima–media regions of the brachial and radial arteries during FMD.[11,12] Furthermore, we have simultaneously measured the stress and strain waveforms noninvasively, and the stress–strain relationship during a heartbeat was identified.[13] In our previous study, from the stress–strain relationship during a heartbeat, the viscoelasticity of the intima–media region was estimated using the least-squares method, and the transient change in viscoelasticity due to FMD was estimated.[14]

In our method, it is necessary to measure the strain waveform using the *phased tracking method*.[15] In this estimation of strain, the lumen–intima boundary (LIB) and media–adventitia boundary (MAB) in an ultrasonic data must be detected. To reduce the operator dependence, it is necessary to detect the LIB and MAB positions objectively on the measured radio frequency (RF) signals. In our previous report, a complex method of template matching between the measured ultrasonic RF signal and the adaptive model signal is proposed for the automatic and objective boundary detection of the radial artery.[11] In this study, we improve the adaptive model and confirm the efficiency of this method by a basic experiment using a rubber sheet. Additionally, the transient changes in the stress–strain relationship and viscoelasticity of the arterial wall should be measured stably for ten minutes. Although the method was previously applied to the longitudinal scan of the arterial wall, it was difficult to maintain an ultrasonic probe in place for ten minutes; thus the scan plane passed through the central axis of the artery. In contrast, there should be a few ultrasonic beams that pass through the central axis of the artery when the artery is measured by a cross-sectional scan. Therefore, for a stable measurement, in this study, the viscoelasticity was measured by a cross-sectional scan of the artery.

2. Principles and Experimental Methods

2.1 Determination of optimum initial positions of artery–wall boundaries

Along an ultrasonic beam around the posterior wall, two dominant ultrasonic echoes are reflected from the LIB and MAB. Ideally, the LIB and MAB are determined by referring to these echoes. However, the MAB is not easily identified because an echo from the MAB includes redundant echoes from the intima–media complex. Therefore, if a simple edge detector, such as a thresholding device, is applied to the ultrasonic RF signals, misdetection frequently occurs owing to the effects of such redundant echoes.

To overcome the disadvantages of conventional gradient methods, Fan *et al.* proposed a technique for the boundary detection of the brachial arterial wall by template matching between an envelope of an ultrasonic RF signal and an

*Research Fellow of the Japan Society for the Promotion of Science.
E-mail address: ikeshita@us.ecei.tohoku.ac.jp

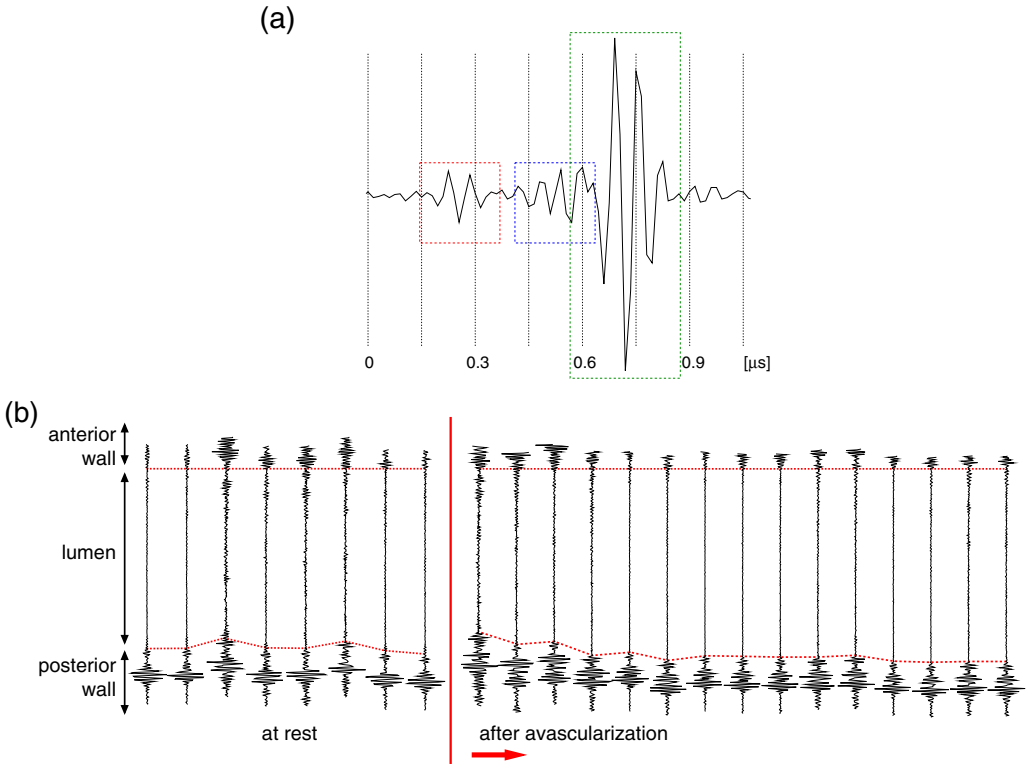

Fig. 1. (Color online) (a) RF echoes from posterior wall of radial artery and (b) the transient change in the RF echoes due to flow-mediated dilation.

adaptive approximate Gaussian model.[16] However, this method detected only the MAB because echoes from the LIB are not always obtained by ultrasonic measurements. In the present study, echoes from the LIB and MAB of the posterior wall should be tracked to accurately obtain the minute change in intima–media thickness. Therefore, it is necessary to detect these boundaries appropriately and objectively. Consequently, in this study, the initial positions of these two boundaries were detected by template matching between the measured RF echoes and the adaptive echo model (not envelope).

Unlike a deterministic signal embedded in a noisy background, the ultrasonic signal from the vessel wall differs from subject to subject, and the waveform of an echo depends on the center frequency and band width of an ultrasonic system. Therefore, a fixed template is not suitable. Figure 1(a) shows RF echoes from the posterior wall of the radial artery, and Fig. 1(b) shows the transient change in the RF echoes due to flow-mediated dilation (FMD). The boundary positions were detected manually on each RF signal, and the RF signals were shown to align the detected LIBs. We refer to these RF echoes to obtain an adaptive template. Echoes from the posterior wall, including redundant echoes from the intima–media complex, are modeled by the sum of three models of a single RF echo. A single RF echo is modeled by multiplying a sinusoidal wave at the center frequency f_0 by a Hanning window $w(t)$, which shows the envelope of an echo, as follows:

$$\hat{z}_i(nT_s) = C_i \cdot \exp[j2\pi f_0(nT_s - \tau_i)] \cdot \omega(nT_s - \tau_i), \quad (1)$$

$$\omega(nT_s) = \begin{cases} 0.5 - 0.5\cos\left(\dfrac{2\pi f_0 nT_s}{N}\right), & (i = 1, 2, 3) \\ 0, \end{cases} \quad (2)$$

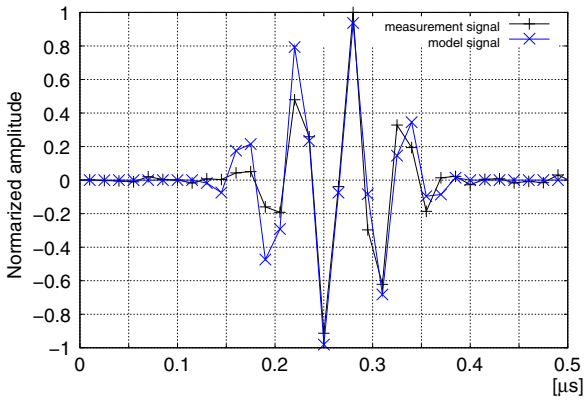

Fig. 2. (Color online) Measured RF echo signal from a point scatterer and model signal.

where $\{C_i\}$ is the amplitude coefficient of the echo, $\{\tau_i\}$ is the time delay of the echo, and n is the number of cycles at the center frequency in an ultrasonic pulse. To obtain complex signals, quadrature demodulation was applied to the measured signal. As shown in Fig. 2, the model echo is in very good agreement with the measured one. The proposed adaptive template echo model $\hat{z}(t)$ is expressed by the linear sum combination of $\{\hat{z}_i(t)\}$ $(i = 1, 2, 3)$, which respectively model echoes reflected from the LIB, the intima–media complex, and the MAB, as follows:

$$\hat{z}(t) = \hat{z}_1(t) + \hat{z}_2(t) + \hat{z}_3(t). \quad (3)$$

First, the center frequency f_0 of each echo is roughly estimated using the discrete Fourier transform, and then it is determined using complex autocorrelation.[17] The parameters $\{C_i\}$ and $\{\tau_i\}$ $(i = 1, 2, 3)$ are determined to obtain a

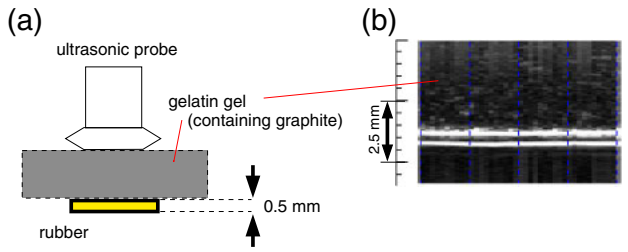

Fig. 3. (Color online) (a) Diagram and (b) B-mode image of the basic experiment.

minimal squared difference between the model $\hat{z}(t)$ and measured echo $z(t)$. The normalized mean squared error (MSE) α is given by

$$\alpha = \frac{\frac{1}{N}\sum_{n=0}^{N-1} |z(nT_s) - \hat{z}(nT_s)|^2}{\frac{1}{N}\sum_{n=0}^{N-1} |z(nT_s)|^2}, \quad (4)$$

where N is the number of samples used for calculating α, and T_s is the sampling interval. According to the above process, the normalized MSE α was calculated with respect to each preassigned $\{\tau_i\}$. The time delay $\{\tau_i\}$ was changed at intervals of $T_s/4$.

Let us describe how the proposed method works. Figures 3(a) and 3(b) show a diagram and a B-mode image of the basic experiment using a rubber sheet. The thickness of the rubber sheet is 0.5 mm, and it includes no scatterers. On the other hand, the gelatin gel containing graphite has some reflection from inside. In this experiment, the reflected complex echo from the anterior boundary, from the gelatin gel to the rubber sheet, imitated the echo from the MAB, including a redundant echo from the intima–media complex, and the single echo from the posterior boundary, from rubber to air, imitated the echo from the LIB. Although the order of these three echo signals is different from that in *in vivo* measurements, the reflected echoes from these two boundaries were estimated to confirm the efficiency of the template matching method.

In this estimation, the echo from the anterior boundary includes the redundant echoes from the gelatin gel. Therefore, in this basic experiment, the model signals are numbered as the redundant echo (z_1), anterior boundary (z_2), and posterior boundary (z_3). The time delay $\{\tau_i\}$ $(i = 1, 2, 3)$ that minimizes the normalized MSE between the measured RF signal and the model signal is determined. In this estimation, anterior and posterior boundaries correspond to the MAB and LIB, respectively. Additionally, the amplitude of the MAB echo is larger than that of the LIB echo in the *in vivo* measurement [for example, Fig. 1(a)]. Therefore, to avoid false boundary detection, the amplitude coefficient C_2 is limited so that $C_1 < C_2$ and $C_3 < C_2$ in the minimization of the MSE. Additionally, the thickness between the anterior and posterior boundaries ranged from 400 to 650 μm. Figure 4(a) shows examples of the detected boundaries on the B-mode image. Figure 4(b) shows the measured echo and a model with a minimal α. In Fig. 4(c), a model of each single echo is shown. The mean of the

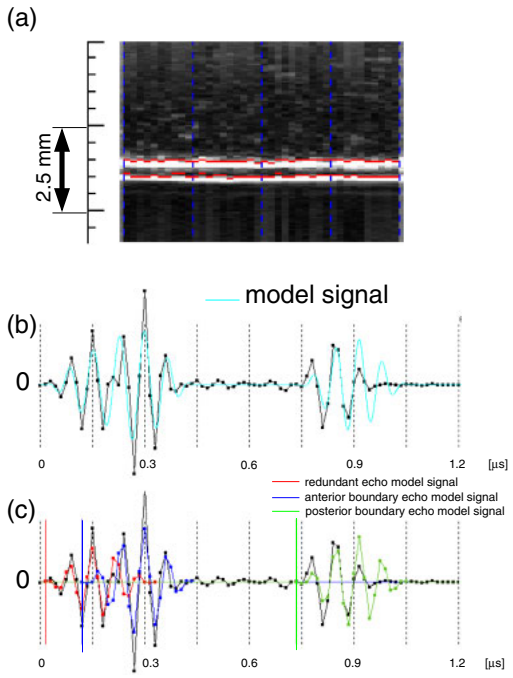

Fig. 4. (Color online) (a) Estimated boundaries on B-mode image. (b) Measured and model signal $\hat{z}$. (c) Model of each single echo $\hat{z}_i$.

estimated thicknesses (corresponding to $\tau_3 - \tau_2$) for ultrasonic beam positions is 453 μm. Additionally, the model echo is in very good agreement with the measured one [normalized MSE is 15.7% in Fig. 4(b)].

In this *in vivo* study, model signals are denoted as the LIB (z_1), redundant echo (z_2), and MAB (z_3), and the distance between the LIB and the MAB (corresponding to $\tau_3 - \tau_1$) ranged from 100 to 400 μm, as determined by referring to the typical intima–media thickness of the arterial wall.[18,19] Additionally, to avoid false boundary detection, the amplitude coefficient C_2 is limited to $C_1 < C_3$ and $C_2 < C_3$ in the *in vivo* measurement, because the amplitude of the MAB echo is much larger than those of the LIB and redundant echoes. The time delay $\{\tau_i\}$ $(i = 1, 2, 3)$ that minimizes the normalized MSE between the measured RF signal and the model signal indicates the optimum positions of the LIB, the redundant echoes from the intima–media complex, and the MAB. The redundant echo was included in the model to avoid the position of the redundant echo from being determined as the position of the MAB.

2.2 Estimation of artery–wall viscoelasticity using the least-squares method

The detailed analysis of the change in the viscoelasticity of the arterial wall due to FMD requires the *in vivo* measurement of the stress–strain relationship, which has not been measured noninvasively thus far.

To determine the stress–strain relationship, the minute change in the thickness (radial strain) $\Delta h(t)$ of the right radial arterial wall during a cardiac cycle was measured using the *phased tracking method*.[15] Together with the measurement of ultrasonic RF signals for the estimation of $\Delta h(t)$, the waveform of blood pressure (stress) $p(t)$ in the left radial artery was continuously measured with a sphygmometer.

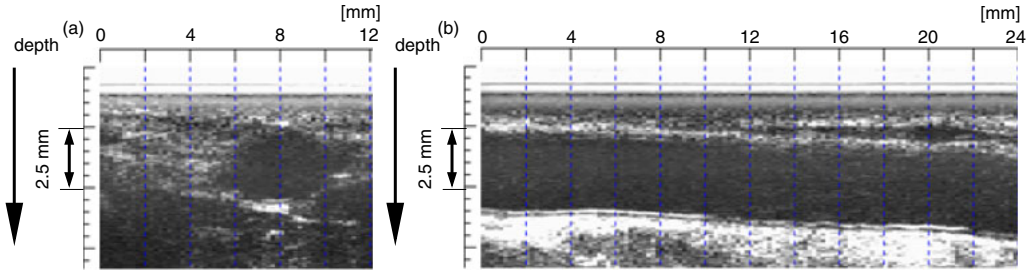

Fig. 5. (Color online) B-mode images of (a) cross-sectional view, and (b) longitudinal view.

To obtain the change in thickness, the velocities of artery–wall boundaries (namely, the LIB and MAB) were estimated. The velocity $v(t)$ was estimated from the phase shift $\widehat{\Delta\theta}(t)$ of echoes in two consecutive frames. The phase shift $\widehat{\Delta\theta}(t)$ was obtained using the complex cross-correlation applied to the quadrature demodulated signals of the measured RF echoes. The change in thickness, $\Delta h(t)$, between two different depths, A and B (corresponding to the LIB and MAB, respectively), in the arterial wall along an ultrasonic beam was obtained from the difference between the displacements $x_{\mathrm{LIB}}(t)$ and $x_{\mathrm{MAB}}(t)$ at these two positions as follows:

$$\Delta\hat{h}(t) = \hat{x}_{\mathrm{LIB}}(t) - \hat{x}_{\mathrm{MAB}}(t) = \int_0^t [\hat{v}_{\mathrm{LIB}}(t) - \hat{v}_{\mathrm{MAB}}(t)]\, dt. \quad (5)$$

The strain $\gamma(t)$ is obtained from the change in thickness, which is divided by the intima–media thickness at the time of the R-wave of the electrocardiogram.

By assuming the Voigt model as a viscoelastic model of the intima–media region, the stress–strain relationship is given by

$$\hat{\tau}(t) = E_{\mathrm{s}}\gamma(t) + \eta\dot{\gamma}(t) + \tau_0, \quad (6)$$

where $\hat{\tau}(t)$ is the stress modeled by the Voigt model, and $\gamma(t)$, $\dot{\gamma}(t)$, E_{s}, and η are the strain, strain rate, static elasticity, and viscosity, respectively. In the *in vivo* measurement, the measured stress $\tau(t)$ is the incremental strain due to the pulse pressure, whereas the measured stress includes the bias stress (diastolic blood pressure). Therefore, τ_0 is added to the right-hand side of eq. (6) as the bias stress corresponding to the diastolic pressure.

The parameters in eq. (6), namely, E_{s}, η, and τ_0, are estimated using the least-squares method by minimizing the mean squared error β between the measured $\tau(t)$ and model $\hat{\tau}(t)$ stresses, which is defined by

$$\beta = E_{\mathrm{t}}\{[\tau(t) - \hat{\tau}(t)]^2\}, \quad (7)$$

where $E_{\mathrm{t}}[\cdot]$ indicates the averaging operation during a cardiac cycle. The parameters $\hat{E}_{\mathrm{s}}$, $\hat{\eta}$, and $\hat{\tau}_0$ that minimize β are determined by setting the partial derivatives of β with respect to E_{s}, η, and τ_0 to zero. To solve the resultant simultaneous equations, the optimum parameters that minimize β are determined.[14)]

2.3 Procedure for *in vivo* measurements

First, the proposed method was applied to the radial, brachial, and carotid arteries to show its feasibility in *in vivo* measurements. In these measurements, ultrasonic RF echoes (transmit center frequency: 22 MHz) were acquired at a sampling frequency of 66.5 MHz for 2 s at a frame rate of about 160 Hz.

Moreover, the right radial artery of a healthy male subject (35 years old) was measured. Together with the measurement of RF signals, the waveform of blood pressure $p(t)$ in the left radial artery was continuously measured with a sphygmometer (Colin Jentow-7700) for the estimation of viscoelasticity.[13,14)] Before the measurement of the transient change in viscoelasticity, the strain and blood pressure waveforms were measured every 1 min for 10 min at rest to evaluate reproducibility. Subsequently, for the measurement of FMD, the measurements of strain and blood pressure were repeated every 20 s for 2 min at rest before avascularization and every 12 s for 3 min after recirculation.

For stable *in vivo* measurements, the radial artery was measured in the cross-sectional view. Figures 5(a) and 5(b) show the B-mode images in the cross-sectional and longitudinal views, respectively. In the cross-sectional view, the LIB can be recognized in five ultrasonic beams (corresponding to a lateral width of about 1 mm). This indicates that the acceptable range of the movement in the direction perpendicular to the arterial longitudinal direction is 1 mm. In the FMD measurement, it is difficult to reduce the movement of an ultrasonic probe or arm to less than 1 mm for 10 min. In the longitudinal scan, a movement in the elevational direction larger than 1 mm makes it impossible to obtain echoes from the LIB at all beam positions. On the other hand, as described above, echoes from the LIB can be obtained at five beams even when the probe or arm moves by more than 1 mm. Therefore, the cross-sectional view is suitable for the measurement of FMD.

3. Results

3.1 Example of template matching for boundary detection of arterial wall

For the validation of the method, we applied template matching to the radial, brachial, and carotid arteries. Figures 6(a), 6(c), and 6(e) show the results of the boundary detection for the radial, brachial, and carotid arteries, respectively. As shown in Fig. 6, the LIB and MAB, which are shown on the B-mode image, are detected appropriately and objectively by the proposed template matching method. Examples of RF signals and the determined echo models are shown in Figs. 6(b), 6(d), and 6(f). The mean squared errors of these results were 13.8, 24.2, and 21.0%, respectively. The echo models are in good agreement with the measured signals.

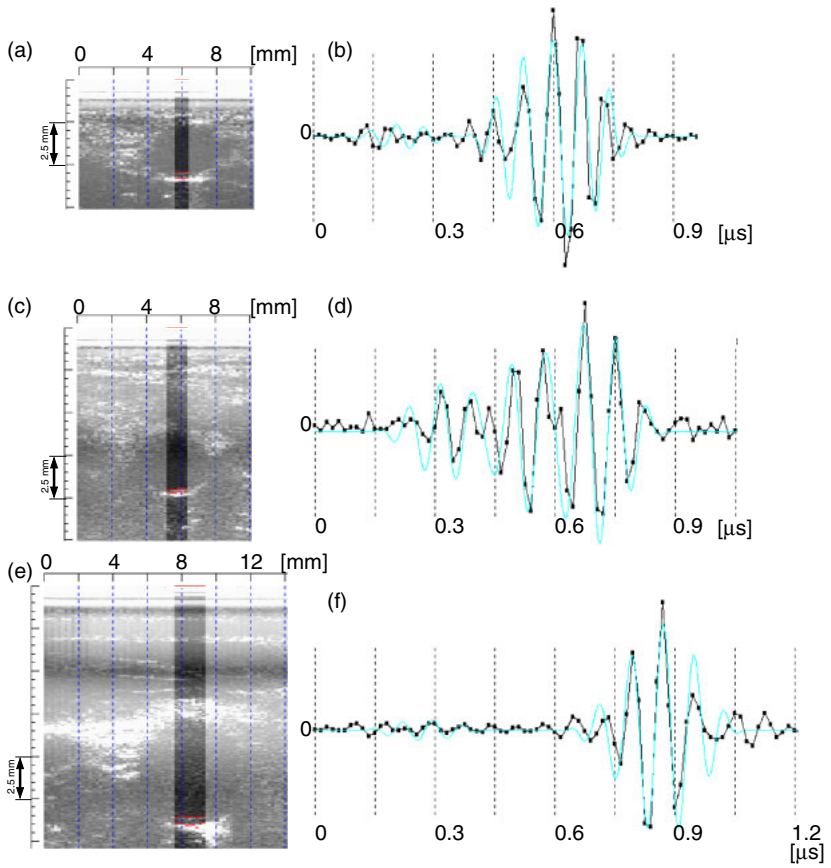

Fig. 6. (Color online) Results of the template matching. (a, c, e) Detected boundaries shown on the B-mode images of the radial, brachial, and carotid arteries, respectively. (b, d, f) Measured RF and model echoes.

3.2 *In vivo* experimental results for healthy subjects

For the evaluation of reproducibility, RF data and the blood pressure waveform at rest were measured every 1 min for 10 min before the measurement of FMD.

Figure 7 shows examples of boundary detection of a radial artery. The LIB and MAB are detected appropriately and objectively. Figure 8 shows the stress–strain relationship obtained using the measured blood pressure $p(t)$ and the change in thickness $\Delta h(t)$ between the detected LIB and MAB. The hysteresis loops are similar to those in our previous reports.[13,14)]

Figure 9 shows the means of the measured static elasticity E_s and viscosity η in the cross-sectional scan. The means were obtained from about 3–5 (cross-sectional scan) available ultrasonic beams. Horizontal dashed lines show the means of all of the respective estimates. The means of the static elasticity E_s and viscosity η are 744 kPa and 1.55 kPa·s in the cross-sectional scan. The measured viscoelasticity was in the same range as that of the carotid artery reported in the literature (*in vitro* measurement).[20)]

Figure 10 shows the transient changes in the means of static elasticity E_s and viscosity η averaged by 3–7 available ultrasonic beams. These parameters were estimated from the stress–strain relationship of the radial artery. The transient change in static elasticity E_s was similar to that in a different elastic parameter reported in the literature.[11,12)] Additionally, including viscosity, the transient changes in these parameters were similar to those in our previous study.[14)] The minimum static elasticity E_s was measured at

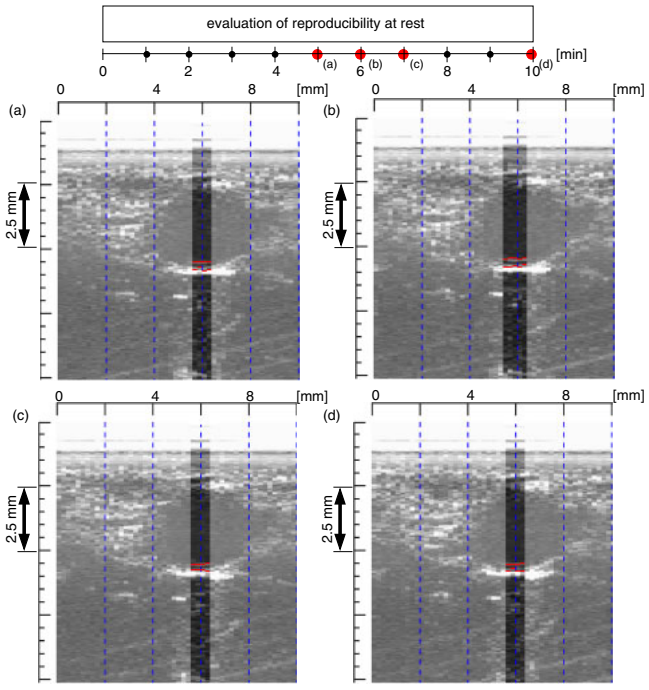

Fig. 7. (Color online) *In vivo* results of the template matching on B-mode images of a radial artery for 10 min.

7 s after the release of the cuff. The maximum % change in static elasticity E_s was about 71.8% (488 kPa). Moreover, the viscosity η, which was evaluated noninvasively by the

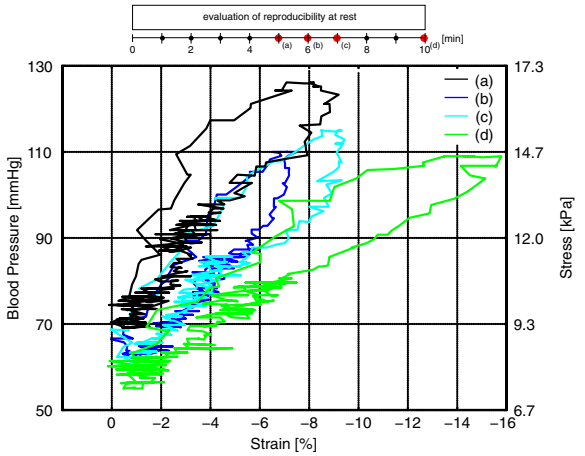

Fig. 8. (Color online) Stress–strain relationships obtained from data in Fig. 7.

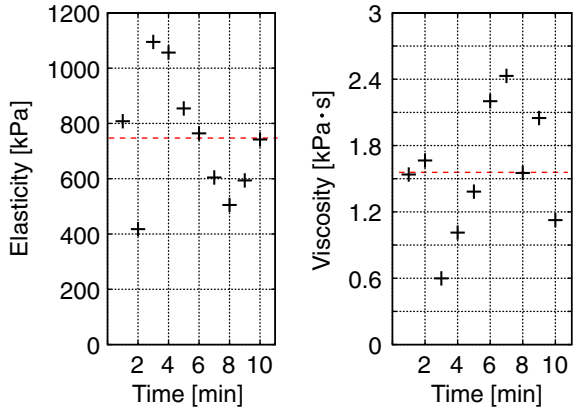

Fig. 9. (Color online) Means of static elasticity E_s and viscosity η of the radial artery for 10 min at rest. Red dashed lines show the means of all of the respective estimates.

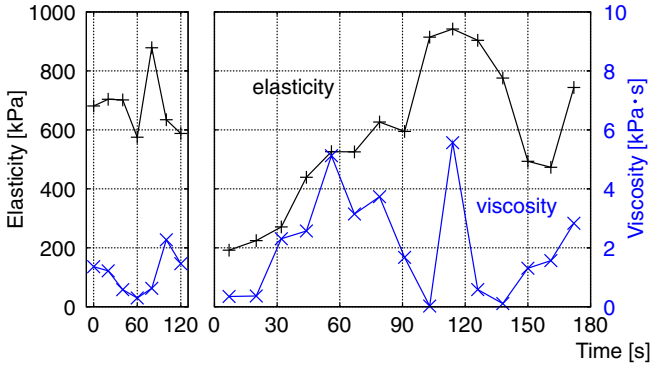

Fig. 10. (Color online) Transient changes in means of estimated static elasticity E_s and viscosity η obtained by boundaries detected using the proposed template matching method.

proposed method, increased after recirculation. The maximum viscosity η at 114 s after recirculation was about 5.6 kPa·s, which is about 398% (4.4 kPa·s) larger than the mean at rest.

For the evaluation of the template matching method, the transient change in viscoelasticity was obtained using the manually detected LIB and MAB. Figure 11 shows the transient changes in the estimated amplitude [Fig. 11(a)], mean squared error [Fig. 11(b)], and the LIB and MAB determined by the proposed method and an operator (referring to B-mode images) [Fig. 11(c)]. In Fig. 11(c), the RF signals obtained at the time of the R-wave of the electrocardiogram are also shown. The LIB positions detected by template matching were similar to those detected by the operator. However, after recirculation, significant differences were observed between the positions detected by template matching and the operator.

Figure 12 shows the transient changes in the static elasticity E_s and viscosity η obtained from the boundaries detected by the operator. The transient changes in static elasticity E_s and viscosity η were similar to those in Fig. 10.

4. Discussion

In this study, we calculated the MSE between the model and measured echoes (not envelope). Figures 6 and 7 show the results of the boundary detection for several ultrasonic beams in a B-mode image in the short axis plane of the radial artery. Although Fig. 6(d) shows an example of ultrasonic echoes in which the boundaries of the arterial wall are difficult to be determined manually, as shown in Fig. 6(c), the boundary positions that are shown as the LIB and MAB on the B-mode image are detected appropriately and objectively by template matching.

Figure 9 shows the means of static elasticity E_s and viscosity η measured every 1 min for 10 min at rest. For a stable measurement, the ultrasonic beam should be perpendicular to the arterial wall and the intima–media region should be visualized clearly during the measurement. In the cross-sectional scan, several ultrasonic beams bisect at right angles, whereas the number of ultrasonic beams, which perpendicularly pass through the artery wall, decreases. However, Fig. 9 shows a large fluctuation in each parameter, even though this method was applied to a healthy subject. Such a fluctuation should be reduced by further investigation.

Figure 10 shows the transient changes in static elasticity and viscosity. The transient changes in these parameters were similar to those in a previous study[14] and to those obtained using the boundaries detected by an operator (Fig. 12). This result shows that the proposed method could detect boundaries automatically and objectively. The temporal decrease in static elasticity E_s and the temporal increase in viscosity η were obtained after recirculation. The measured temporal change in viscoelasticity suggests that this method is able to measure the temporal change in the mechanical property of the arterial wall due to FMD, although the physiological meanings of such temporal changes and recoveries of E_s and η should be further investigated.

Figure 11(c) shows the LIB and MAB detected by template matching and an operator (referring to B-mode images). Just after recirculation, there are significant differences between the positions detected by template matching and the operator. Although there are small fluctuations in MSE and the estimated amplitude of echoes in Figs. 11(a) and 11(b), they are similar just after recirculation. However, at the time of 161 s after recirculation, the estimated amplitudes of echoes are similar, but

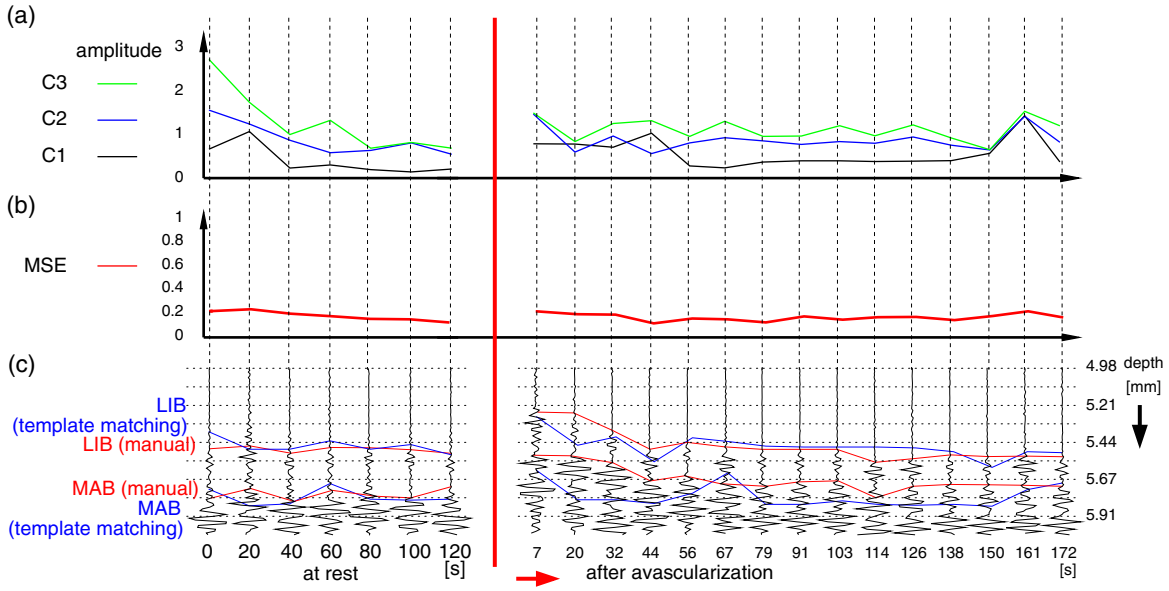

Fig. 11. (Color online) (a) Transient changes in the estimated amplitude, (b) mean squared error, and (c) boundaries determined by the proposed method and an operator.

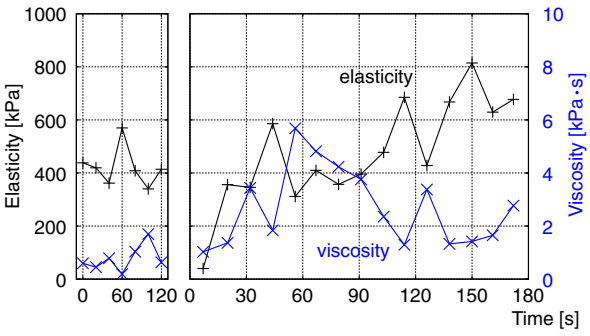

Fig. 12. (Color online) Transient changes in means of estimated static elasticity E_s and viscosity η obtained using boundaries detected manually.

there is a small difference between the boundaries detected by template matching and the operator. Therefore, it is necessary to reveal the origin of the redundant echo.

As described above, there are many aspects of this study that should be further investigated. However, the boundaries were detected objectively and automatically by the proposed template matching method, and the obtained results show that the method described in this paper can detect changes in the viscoelastic properties of the arterial wall due to FMD. Such a method would be beneficial for the detection of early-stage atherosclerosis.

5. Conclusions

In this study, for an accurate and stable measurement of transient change in viscoelasticity, we applied the proposed template matching method between the measured RF and adaptive model signals for the boundary detection of the artery. The proposed template matching method showed a potential for the accurate boundary detection and stable analysis of the transient changes in the mechanical properties of the intima–media region caused by FMD.

Acknowlegment

This work was supported by a Grant-in-Aid for JSPS Fellows.

1) R. Ross: New Engl. J. Med. **340** (1999) 115.
2) M. Walski, S. Chlopicki, R. Celary-Walska, and M. Frontczak-Baniewicz: J. Physiol. Pharmacol. **53** (2002) 713.
3) Y. Matsuzawa: Nippon Rinsho **51** (1993) 1951 [in Japanese].
4) P. M. Vanhoutte: J. Clin. Invest. **107** (2001) 23.
5) D. S. Celermajer, K. E. Soresen, V. M. Gooch, D. J. Spiegelhalter, O. I. Miller, J. D. Sullivan, J. K. Lloyd, and J. E. Deanfield: Lancet **340** (1992) 1111.
6) M. C. Corretti, T. J. Anderson, E. J. Benjamin, D. Celermajer, F. Charbonneau, M. A. Creager, J. Deanfield, H. Drexler, M. Gerhard-Herman, D. Herrington, P. Vallance, J. Vita, and R. Vogel: J. Am. Coll. Cardiol. **39** (2002) 257.
7) J. Deanfield, A. Donald, C. Ferri, C. Giannattasio, J. Halcox, S. Halligan, A. Lerman, G. Mancia, J. J. Oliver, A. C. Pessina, D. Rizzoni, G. P. Rossi, A. Salvetti, E. L. Schiffrin, S. Taddei, and D. J. Webb: J. Hypertension **23** (2005) 7.
8) N. M. De Roos, M. L. Bots, E. G. Schouten, and M. B. Katan: Ultrasound Med. Biol. **29** (2003) 401.
9) M. Nishino: Cho-onpa Igaku **37** (2010) 243 [in Japanese].
10) A. S. Kelly, D. R. Kaiser, D. R. Dengel, and A. J. Bank: Ultrasound Med. Biol. **30** (2004) 1447.
11) T. Kaneko, H. Hasegawa, and H. Kanai: Jpn. J. Appl. Phys. **46** (2007) 4881.
12) M. Sugimoto, H. Hasegawa, and H. Kanai: Jpn. J. Appl. Phys. **44** (2005) 6297.
13) K. Ikeshita, H. Hasegawa, and H. Kanai: Jpn. J. Appl. Phys. **47** (2008) 4165.
14) K. Ikeshita, H. Hasegawa, and H. Kanai: Jpn. J. Appl. Phys. **48** (2009) 07GJ10.
15) H. Kanai, M. Sato, Y. Koiwa, and N. Chubachi: IEEE Trans. Ultrason. Ferroelectr. Freq. Control **43** (1996) 791.
16) L. Fan, P. Santago, W. Riley, and D. M. Herrington: Ultrasound Med. Biol. **27** (2001) 399.
17) S. I. Rabben, S. Bjærum, V. Sørhus, and H. Torp: Ultrasound Med. Biol. **28** (2002) 507.
18) T. Furumoto, S. Fujii, K. Hishihara, S. Yamada, K. Komuro, K. Goto, H. Onozuka, T. Mikami, A. Kitabatake, and B. E. Sobel: Am. J. Cardiol. **93** (2004) 997.
19) D. P. Germain, P. Boutouryrie, B. Laloux, and S. Laurent: Arterioscler. Thromb. Vasc. Biol. **23** (2003) 836.
20) B. M. Learoyd and M. G. Taylor: Circ. Res. **18** (1966) 278.